The influence of baffle fairings on the acoustic performance of rectangular splitter silencers

Ray Kirby

School of Engineering and Design,

Mechanical Engineering,

Brunel University, Uxbridge, Middlesex, UB8 3PH, UK.

ABSTRACT

A numerical model based on the finite element method is developed for a finite length, HVAC splitter silencer. The model includes an arbitrary number of bulk-reacting splitters separated from the airway by a thin perforated metal sheet and accommodates higher order modes in the incident sound field. Each perforated sheet is joined to rigid, impervious, metallic fairing situated at either end of a splitter. The transmission loss for the silencer is quantified by application of the point collocation technique, and predictions are compared to experimental measurements reported in the literature. The splitter fairing is shown to significantly affect silencer performance, especially when higher order incident modes are present. It is concluded that laboratory measurements, and theoretical predictions, that are based on a predominantly plane wave sound source are unlikely to reflect accurately the true performance of an HVAC silencer in a real ducting system.

I. INTRODUCTION

Dissipative silencers are commonly used in HVAC ducts to attenuate broadband noise emanating from an air moving device such as a fan. HVAC ducts commonly have a rectangular crosssection and a silencer made up of a number of parallel splitters. Each splitter normally consists of a bulk reacting porous material separated from the airway by a thin, perforated, metal sheet. Each perforated sheet is joined to metallic fairing at either end of the splitter (see Fig. 1). This helps to maintain the dimensional stability of a splitter, but also to channel airflow between each splitter, lowering the static air pressure loss across the silencer. Each section of fairing will, however, also affect the propagation of sound through the silencer by modifying the acoustic end correction at the inlet and outlet planes of the silencer. The influence of this fairing on the overall performance of a splitter silencer has largely been ignored in the literature, and so the aim of this paper is to investigate the effect of splitter fairing on HVAC silencer performance.

The effect on silencer performance of splitter fairing is normally assumed to be negligible. Moreover, the majority of theoretical studies on HVAC splitters are limited to computing modal attenuation in an infinite duct. For example, Cummings [1] quantified the attenuation of the first few least attenuated modes in a rectangular duct lined on opposite walls; Bies *et al.* [2] report general design curves for rectangular ducts lined on opposite walls, computed using the least attenuated mode; and Kakoty and Roy [3] examined infinite rectangular ducts lined on all four walls. The methods of Cummings and Sormaz [4], and Astley and Cummings [5], are both capable of examining a large number of higher-order modes in a silencer that contains an arbitrary number of splitters, although both techniques are, again, restricted to infinite ducts.

Computing only modal attenuation suppresses the effects of acoustic scattering at either end of a silencer. To date, attempts to quantify end effects for bulk reacting HVAC silencers have been restricted to the specification of simplistic end correction factors. For example, Ramakrishnan and Watson [6] derive heuristic end correction factors by summing the decay rate of individual modes; Ramakrishnan and Stevens [7] use an expression developed by Beranek [8] for a plane wave expansion chamber; and Brandstätt *et al.* [9] generate transmission loss curves by comparing predicted modal attenuation with a large number of experimental measurements. Clearly, these methods do not fully characterise silencer end effects, nor are they likely to be applicable over a wide range of silencer parameters, including a silencer with a large number of splitters. In fact, end effects for bulk reacting splitter silencers have only recently been quantified by Kirby and Lawrie [10], who demonstrated excellent agreement between numerical point collocation predictions and those found using an exact analytic approach. Kirby and Lawrie studied large HVAC silencers but the results were restricted to three splitters, and the effects of a perforate and splitter fairing were omitted. The addition of splitter fairing for a bulk reacting material has yet to be considered, although Mechel [11, 12] did include fairings in a study of locally reacting splitters. The assumption of a locally reacting absorbent does, however, reduce the applicability of Mechel's technique, as it assumes either a relatively thin splitter, when compared to the overall duct dimensions, or a porous material of very high flow resistivity: neither case is likely to exist in most splitter silencer applications.

A numerical model aimed at quantifying the acoustic performance of a finite length splitter silencer is presented here. Included are the effects of a perforated sheet separating a bulk

reacting material from the airway, an impervious fairing at either end of a splitter, and an arbitrary number of splitters making up the silencer. The silencer is assumed to have a uniform cross-section and the effects of mean flow are neglected. To accommodate relatively large HVAC ducts, which are common in practice, a multi-modal sound field is chosen to excite the silencer. The effects of the splitter fairing are quantified by comparison with transmission loss predictions reported by Kirby and Lawrie [10] (who omit splitter end baffles), and with experimental results reported by Mechel [12]. The effects of varying both the porosity of the perforate, and the properties of the bulk reacting porous material, are also investigated.

II. THEORY

The analysis proceeds by assuming that the acoustic fields in the inlet/outlet ducts, and also the silencer section, may be expanded as an infinite sum over the duct/silencer eigenmodes. On finding the duct/silencer eigenfunctions and associated wave numbers, the modal amplitudes may be computed by application of the axial matching conditions, after suitable truncation of each modal sum. A numerical approach similar to the one described by Kirby [13], and Kirby and Lawrie [10], is adopted here and so, after introducing the duct geometry and governing wave equations, a finite element eigenvalue analysis is described; this is followed by a point collocation scheme that seeks to fulfil the axial continuity conditions.

A. Geometry and governing equations

An arbitrary number of bulk reacting splitters are shown in Fig. 1. A multi-mode sound source, propagating in the positive x direction in region R_1, is used to excite the silencer. The duct is

terminated anechoically in region R_4. The duct walls in regions R_1 and R_4 are assumed to be rigid and impervious to sound. Each splitter has a length L and is terminated at $x = 0$, and $x = L$, by a metallic fairing that is assumed to be rigid and impervious to sound propagation, and also of negligible thickness when compared to the overall silencer dimensions. Each splitter contains a bulk reacting porous material that is separated from the airway by a perforated sheet. A different porous material is assumed to be present in each splitter, although the material is assumed to be both homogeneous and isotropic. Furthermore, a different perforate sheet may be present on either side of a splitter, provided that the properties of the perforate remain uniform over $0 \le x \le L$, and $0 \le z \le H$. The duct walls (at $y = 0$, and $y = b$, over $0 \le z \le H$; and $z = 0$, and $z = H$, over $0 \le y \le b$) are assumed to be rigid and impervious to sound propagation for $0 \le x \le L$. A total of s splitters are depicted in Fig. 1: each splitter has a width d and is separated from the following splitter by an airway of width h. It is convenient to combine each section of airway, and to denote region R_2 as,

$$R_2 = A_1 + A_2 + A_3 + ... + A_{s-2} + A_{s-1}. \tag{1}$$

For each splitter,

$$R_3 = B_1 + B_2 + B_3 + ... + B_{s-1} + B_s. \tag{2}$$

In addition, region R_c consists of the airway, region R_2, added to the porous material, region R_3. The acoustic wave equation for the inlet duct region R_1, the outlet duct region R_4, and the airway region R_2, is given by

$$\frac{1}{c_0^2}\frac{D^2 p_q'}{Dt^2} - \nabla^2 p_q' = 0, \tag{3}$$

where c_0 is the isentropic speed of sound in air, p'_q is the acoustic pressure in region q (where $q = 1, 2, \text{or } 4$), and t is time. For the porous material, the acoustic wave equation for any splitter k, is given by

$$\frac{1}{c_k^2}\frac{D^2 p'_k}{Dt^2} - \nabla^2 p'_k = 0, \tag{4}$$

where c_k is the speed of sound in the porous material. The acoustic field in each region is expanded as an infinite sum over the duct eigenmodes, to give

$$p'_1(x,y,z;t) = \sum_{j=0}^{\infty} F_j \Phi_j(y,z) e^{\mathrm{i}(\omega t - k_0 \gamma_j x)} + \sum_{j=0}^{\infty} A_j \Phi_j(y,z) e^{\mathrm{i}(\omega t + k_0 \gamma_j x)}, \tag{5}$$

$$p'_c(x,y,z;t) = \sum_{m=0}^{\infty} B_m \Psi_m(y,z) e^{\mathrm{i}(\omega t - k_0 \lambda_m x)} + \sum_{m=0}^{\infty} C_m \Psi_m(y,z) e^{\mathrm{i}(\omega t + k_0 \lambda_m x)}, \tag{6}$$

$$p'_4(x,y,z;t) = \sum_{n=0}^{\infty} D_n \Phi_n(y,z) e^{\mathrm{i}(\omega t - k_0 \gamma_n x')}. \tag{7}$$

Here, A_j, B_m, C_m, D_n, and F_j are modal amplitudes, λ_m is the wavenumber in region R_c, and γ_j is the wavenumber in the inlet/outlet section. The quantities $\Phi_j(y,z)$ and $\Psi_m(y,z)$ are the transverse duct eigenfunctions in the inlet/outlet region and the silencer section respectively. In addition, $\mathrm{i} = \sqrt{-1}$, $k_0 = \omega / c_0$, and ω is the radian frequency. Note that p'_c encompasses regions R_2 and R_3, so that λ is the (coupled) axial wavenumber for the silencer section.

B. Finite element eigenvalue analysis

A finite element eigenvalue analysis is carried out over the cross section of both the inlet/outlet ducts and the silencer section, although the analysis for an unlined rectangular duct is straightforward and so is not reported here. For the silencer section (region R_c) the assumed form for p_c' [Eq. (6)] is substituted into Eq. (3), and this yields, for mode *m* and airway section *r*,

$$\nabla_{yz}^2 \psi_r(y,z) + k_0^2\left[1-\lambda^2\right]\psi_r(y,z) = 0\,, \tag{8}$$

where $\psi_r(y,z)$ is the component of eigenfunction $\Psi(y,z)$ that lies in region A_r (see Fig. 1). Here, ∇_{yz} denotes a two-dimensional form of the Laplacian operator in the (*y*, *z*) plane. For mode *m*, the wave equation in splitter *k* yields,

$$\nabla_{yz}^2 \varphi_k(y,z) + k_0^2\left[\Gamma_k^2-\lambda^2\right]\varphi_k(y,z) = 0\,. \tag{9}$$

Here, $\varphi_k(y,z)$ is the component of the eigenfunction $\Psi(y,z)$ that lies in region B_k, and Γ_k is the (dimensionless) propagation constant of the porous material in splitter *k*. The eigenfunction in each region may be approximated by a trial solution of the form

$$\psi_r(y,z) = \sum_{j=1}^{n_r} N_{rj}(y,z)\psi_{rj}\,, \tag{10}$$

and

$$\varphi_k(y,z) = \sum_{n=1}^{n_k} G_{kn}(y,z)\varphi_{kn}\,. \tag{11}$$

Here, $N_{rj}(y,z)$ and $G_{kn}(y,z)$ are the global trial (or shape) functions for the finite element mesh in airway *r* and splitter *k*, respectively; the number of nodes in airway *r* is n_r, and in splitter *k* is n_k. It is convenient to express these nodal values in vector form, and to number the nodes as follows: for airway *r*,

$$\psi_r(y,z) = \left[N_{r1}(y,z), N_{r2}(y,z), ..., N_{rn_r}(y,z)\right] \begin{bmatrix} \psi_{r1} \\ \psi_{r2} \\ \psi_{rn_r} \end{bmatrix} = \mathbf{N}_r \mathbf{\Psi}_{r2}, \tag{12}$$

and for splitter *k*,

$$\varphi_k(y,z) = \left[G_{k1}(y,z), G_{k2}(y,z), ..., G_{kn_k}(y,z)\right] \begin{bmatrix} \varphi_{k1} \\ \varphi_{k2} \\ \varphi_{kn_k} \end{bmatrix} = \mathbf{G}_k \mathbf{\Psi}_{k3}. \tag{13}$$

The nodal values for each airway and splitter are combined to give,

$$\mathbf{\Psi}_2 = \left[\mathbf{\Psi}_{12} \quad \mathbf{\Psi}_{22} \quad \mathbf{\Psi}_{32} .... \mathbf{\Psi}_{(s-1)2}\right]^{\mathrm{T}}, \text{ and } \mathbf{\Psi}_3 = \left[\mathbf{\Psi}_{13} \quad \mathbf{\Psi}_{23} \quad \mathbf{\Psi}_{33} ..... \mathbf{\Psi}_{s3}\right]^{\mathrm{T}}. \tag{14a, b}$$

The appropriate boundary conditions for regions R_2 and R_3 are zero normal acoustic particle velocity on the walls of the silencer, continuity of normal particle velocity over each perforate, and a pressure condition over each perforate. Accordingly, zero normal particle velocity for airway *r* gives

$$\frac{\partial \psi_r}{\partial z}(y,0) = 0, \text{ and } \frac{\partial \psi_r}{\partial z}(y,H) = 0, \qquad y \in R_2. \tag{15}$$

For splitter *k*,

$$\frac{\partial \varphi_k}{\partial z}(y,0) = 0 \text{, and } \frac{\partial \varphi_k}{\partial z}(y,H) = 0 \text{,} \qquad y \in R_3 \text{.} \tag{16}$$

For the side walls,

$$\frac{\partial \varphi_1}{\partial y}(b,z) = 0 \text{, and } \frac{\partial \varphi_s}{\partial y}(0,z) = 0 \text{,} \qquad 0 \le z \le H \text{.} \tag{17}$$

Each splitter has a perforate located on both sides, except for those splitters located on the wall of the duct; thus for splitter k $(1 \le k \le s)$, continuity of normal particle velocity over a perforate yields,

$$\frac{\partial \psi_{k-1}}{\partial y}(y_{2k-2}^-, z) = -\frac{\rho_0}{\rho_k(\omega)} \frac{\partial \varphi_k}{\partial y}(y_{2k-2}^+, z), \qquad 0 \le z \le H \text{ ; } k \ne 1 \text{ ,} \tag{18}$$

and

$$\frac{\partial \psi_k}{\partial y}(y_{2k-1}^-, z) = -\frac{\rho_0}{\rho_k(\omega)} \frac{\partial \varphi_k}{\partial y}(y_{2k-1}^+, z), \qquad 0 \le z \le H \text{ ; } k \ne s \text{.} \tag{19}$$

Similarly, the pressure condition over each perforate yields

$$\psi_{k-1}(y_{2k-2}^-, z) - \varphi_k(y_{2k-2}^+, z) = \frac{\mathrm{i}\zeta_{2k-2}}{k_0} \frac{\partial \psi_{k-1}}{\partial y}(y_{2k-2}^-, z), \qquad 0 \le z \le H \text{ ; } k \ne 1 \text{ ,} \tag{20}$$

and

$$\psi_k(y_{2k-1}^-, z) - \varphi_k(y_{2k-1}^+, z) = \frac{\mathrm{i}\zeta_{2k-1}}{k_0} \frac{\partial \psi_k}{\partial y}(y_{2k-1}^-, z), \qquad 0 \le z \le H \text{ ; } k \ne s \text{ .} \tag{21}$$

Here, the (dimensionless) acoustic impedance of perforate e is denoted ζ_e, the mean fluid density in region R_2 is ρ_0, and $\rho_k(\omega)$ is the equivalent complex density of the porous material in splitter k. Equations (18)-(21) assume the thickness of the perforate is negligible. Each perforate is numbered according to its location so that perforate 1 is located at y_1, and lies between splitter

B_1 and airway A_1; perforate 2 is located at y_2, and lies between splitter B_2 and airway A_1; perforate 3 is located at y_3, and lies between splitter B_2 and airway A_2; and so on. Thus, the location of each perforate is given as

$$y_{2k-2} = \sum_{i=1}^{k-1} (d_i + h_i), \qquad 1 < k \le s, \tag{22}$$

and

$$y_{2k-1} = \sum_{i=1}^{k} d_i + \sum_{j=1}^{k-1} h_j, \qquad 1 \le k < s. \tag{23}$$

Here, d_k is the width of splitter k, and h_r is the width of airway r (see Fig. 1). Note that each perforate has been numbered individually to allow a different sheet to be placed on either side of a splitter. Furthermore, finite element discretisation requires the specification of two nodes at a given location on a perforate: one node which belongs only to the mesh in the airway, and one only to the mesh in the absorbent. Here, a node at the perforate but lying in the airway is said to have location y^-; a node at the perforate but lying in the absorbent is said to have location y^+.

The boundary conditions specified in Eqs. (15)-(21) may be combined with Eqs. (8) and (9) to give a governing eigenequation for the silencer. The details of the weak Galerkin finite element formulation for this type of problem have been reported elsewhere [5, 13], and so only the final eigenequation is presented here:

$$\left[[\mathbf{A}] + \lambda^2 [\mathbf{B}]\right]\{\mathbf{\Psi}\} = \{\mathbf{0}\}, \tag{24}$$

where $\mathbf{\Psi} = \left[\mathbf{\Psi}_2 \quad \mathbf{\Psi}_3\right]^{\mathrm{T}}$, and

$$[\mathbf{A}]\{\boldsymbol{\Psi}\} = [\mathbf{C}]\{\boldsymbol{\Psi}_2\} + [\mathbf{D}]\{\boldsymbol{\Psi}_3\}, \tag{25}$$

$$[\mathbf{B}]\{\boldsymbol{\Psi}\} = k_0^2[\mathbf{M}_2]\{\boldsymbol{\Psi}_2\} + k_0^2[\mathbf{M}_3]\{\boldsymbol{\Psi}_3\}. \tag{26}$$

Here,

$$[\mathbf{C}] = [\mathbf{K}_2] - k_0^2[\mathbf{M}_2] + ik_0\left([\mathbf{M}_2^-] - [\mathbf{M}_3^+]\right). \tag{27}$$

and,

$$[\mathbf{D}] = [\mathbf{K}_3] + k_0^2[\mathbf{M}_3] - ik_0\left([\mathbf{M}_2^-] - [\mathbf{M}_3^+]\right). \tag{28}$$

For the airway,

$$[\mathbf{K}_2] = \begin{bmatrix} [\mathbf{K}_{12}] & \mathbf{0} & \cdots & \mathbf{0} \\ \mathbf{0} & [\mathbf{K}_{22}] & \cdots & \mathbf{0} \\ \vdots & \vdots & \ddots & \vdots \\ \mathbf{0} & \mathbf{0} & \cdots & [\mathbf{K}_{(s-1)2}] \end{bmatrix}, \tag{29}$$

and

$$[\mathbf{K}_{r2}] = \int_{A_r} \nabla_{yz} N_{ri}(y,z) \cdot \nabla_{yz} N_{rj}(y,z)\, dydz, \qquad i = 1,...,n_r;\ j = 1,...,n_r. \tag{30}$$

In addition,

$$[\mathbf{M}_2] = \begin{bmatrix} [\mathbf{M}_{12}] & \mathbf{0} & \cdots & \mathbf{0} \\ \mathbf{0} & [\mathbf{M}_{22}] & \cdots & \mathbf{0} \\ \vdots & \vdots & \ddots & \vdots \\ \mathbf{0} & \mathbf{0} & \cdots & [\mathbf{M}_{(s-1)2}] \end{bmatrix}, \tag{31}$$

and,

$$[\mathbf{M}_{r2}] = \int_{A_r} N_{ri}(y,z) \cdot N_{rj}(y,z)\, dydz; \qquad i = 1,...,n_r;\ j = 1,...,n_r. \tag{32}$$

For the absorbent,

$$[\mathbf{K}_3]=\begin{bmatrix}[\mathbf{K}_{13}] & \mathbf{0} & \cdots & \mathbf{0}\\ \mathbf{0} & [\mathbf{K}_{23}] & \cdots & \mathbf{0}\\ \vdots & \vdots & \ddots & \vdots\\ \mathbf{0} & \mathbf{0} & \cdots & [\mathbf{K}_{(s-1)3}]\end{bmatrix}, \tag{33}$$

where,

$$[\mathbf{K}_{k3}]=\int_{B_k}\nabla_{yz}G_{ki}(y,z)\cdot\nabla_{yz}G_{kj}(y,z)\,dydz, \qquad i=1,...,n_k;\ j=1,...,n_k. \tag{34}$$

In addition,

$$[\mathbf{M}_3]=\begin{bmatrix}[\mathbf{M}_{13}] & \mathbf{0} & \cdots & \mathbf{0}\\ \mathbf{0} & [\mathbf{M}_{23}] & \cdots & \mathbf{0}\\ \vdots & \vdots & \ddots & \vdots\\ \mathbf{0} & \mathbf{0} & \cdots & [\mathbf{M}_{(s-1)3}]\end{bmatrix}, \tag{35}$$

where,

$$[\mathbf{M}_{k3}]=\Gamma_k^2\int_{B_k}G_{ki}(y,z)\cdot G_{kj}(y,z)\,dydz, \qquad i=1,...,n_k;\ j=1,...,n_k. \tag{36}$$

For each node in the finite element mesh that lies on a perforate but belongs to the airway,

$$[\mathbf{M}_2^-]=\begin{bmatrix}[\mathbf{M}_{12}^-] & \mathbf{0} & \cdots & \mathbf{0}\\ \mathbf{0} & [\mathbf{M}_{22}^-] & \cdots & \mathbf{0}\\ \vdots & \vdots & \ddots & \vdots\\ \mathbf{0} & \mathbf{0} & \cdots & [\mathbf{M}_{(s-1)2}^-]\end{bmatrix}, \tag{37}$$

and,

$$[\mathbf{M}_{r2}^-]=\begin{bmatrix}\mathbf{Q}_r^- & \mathbf{0}\\ \mathbf{0} & \mathbf{T}_r^-\end{bmatrix}. \tag{38}$$

Here,

$$\left[\mathbf{Q}_r^-\right]=\frac{1}{\zeta_{2r-1}}\int_0^H N_{ri}(y_{2r-1}^-,z)\cdot N_{rj}(y_{2r-1}^-,z)\,dz\,,\qquad i=1,...,n_r;\ j=1,...,n_r\,. \tag{39}$$

and

$$\left[\mathbf{T}_r^-\right]=\frac{1}{\zeta_{2r}}\int_0^H N_{ri}(y_{2r}^-,z)\cdot N_{rj}(y_{2r}^-,z)\,dz\,,\qquad i=1,...,n_r;\ j=1,...,n_r\,. \tag{40}$$

Similarly, for each node in the finite element mesh that lies on a perforate but belongs to the absorbent,

$$\left[\mathbf{M}_3^+\right]=\begin{bmatrix}\left[\mathbf{M}_{13}^+\right] & \mathbf{0} & \cdots & \mathbf{0}\\ \mathbf{0} & \left[\mathbf{M}_{23}^+\right] & \cdots & \mathbf{0}\\ \vdots & \vdots & \ddots & \vdots\\ \mathbf{0} & \mathbf{0} & \cdots & \left[\mathbf{M}_{(s-1)3}^+\right]\end{bmatrix}, \tag{41}$$

and,

$$\left[\mathbf{M}_{k3}^+\right]=\begin{bmatrix}\mathbf{Q}_k^+ & \mathbf{0}\\ \mathbf{0} & \mathbf{T}_k^+\end{bmatrix}. \tag{42}$$

Here,

$$\left[\mathbf{Q}_k^+\right]=\frac{\rho_k(\omega)}{\rho_0\zeta_{2k-2}}\int_0^H N_{ki}(y_{2k-2}^+,z)\cdot N_{kj}(y_{2k-2}^+,z)\,dz\,,\quad i=1,...,n_k;\ j=1,...,n_k\text{, for } 1<k\le s\,, \tag{43}$$

and

$$\left[\mathbf{T}_k^+\right]=\frac{\rho_k(\omega)}{\rho_0\zeta_{2k-1}}\int_0^H N_{ki}(y_{2k-1}^+,z)\cdot N_{kj}(y_{2k-1}^+,z)\,dz\,,\quad i=1,...,n_k;\ j=1,...,n_k\text{; for } 1\le k<s\,. \tag{44}$$

Here it is assumed that identical elements are chosen on either side of the perforate. The non zero elements of matrices $\left[\mathbf{M}_2^-\right]$ and $\left[\mathbf{M}_3^+\right]$ that appear in Eq. (25) are limited to those nodes lying on a perforate, although for convenience Eqs. (39), (40), (43), and (44) are written in general form.

Finally, Eq. (24) may be re-written as

$$\left[-[\mathbf{B}]^{-1}[\mathbf{A}]\right]\{\mathbf{\Psi}\} = \lambda^2\{\mathbf{\Psi}\}, \tag{45}$$

and is solved for the axial wave number λ, which yields N_c eigenvalues and associated eigenvectors, where $N_c = N_2 + N_3$. Here, $N_2 = \sum_{r=1}^{s-1} n_r$, and $N_3 = \sum_{k=1}^{s} n_k$, so that N_2 is the number of nodes in the airway, N_3 the number of nodes in the absorbent.

C. Numerical matching of sound fields

On obtaining the eigenfunctions and wave numbers for regions R_1, R_c and R_4, the axial matching conditions are enforced over planes A and B using point collocation. The appropriate matching conditions (at $x = 0$ and $x = L$) are continuity of acoustic pressure and normal particle velocity over the airway, and zero normal acoustic velocity over each splitter fairing. The most convenient approach to enforcing these matching conditions, and the one adopted by Kirby and Lawrie [10], is to choose an identical transverse finite element mesh in regions R_1, R_c and R_4 and to match over every common node. However, the addition of a perforate complicates matters, as additional nodes in the transverse finite element mesh are required at each perforate location in the silencer section. For an automotive silencer, Kirby [13] addressed this problem by separately

matching pressure and velocity at a node in the airway region (location y^-) and normal particle velocity at a node in the absorbent region (location y^+). For example, in Fig. 2(a) node *b* is said to have location y^- (position is exaggerated in the diagram, and for clarity only one dimension is shown), so that pressure and velocity conditions are enforced between nodes *a* and *b*. For node *c* (location y^+), matching conditions appropriate to the absorbent region only are enforced – in this case zero normal particle velocity. For the splitters in the current study, a further complication arises from the presence of the splitter fairings. For example, in Fig. 2(b) the location of nodes *a* and *j* (again, exaggerated in the diagram) is no longer certain as they could assume either a y^- or a y^+ location. A solution is to choose the location of y^- for nodes *a* and *j*, and to apply matching conditions appropriate to the airway region between nodes *a* and *b*, and nodes *j* and *l*. Similarly, nodes *c* and *k*, in region R_c, are chosen to lie in a y^+ location, and zero normal particle velocity is applied at the fairing in the absorbent region. Thus, zero axial particle velocity is enforced over the fairing in region R_1 by using nodes *d*, *f* and *h* in Fig. 2b. In general terms, therefore, a reduction in the number of matching locations takes place in region R_1, although this reduction serves to compensate exactly for the discrepancy between the number of nodes in region R_1 (or R_4) and region R_c. Note, this will not reduce the accuracy of the method, when compared to the method of Kirby and Lawrie [10], since the mesh density in each region is not reduced: instead, nodes are added to account for the presence of a perforate.

For the airway, continuity of pressure over plane A yields

$$\sum_{j=0}^{N_1} F_j \mathbf{\Phi}_{2j} + \sum_{j=0}^{N_1} A_j \mathbf{\Phi}_{2j} = \sum_{m=0}^{N_c} B_m \mathbf{\Psi}_{2m} + \sum_{m=0}^{N_c} C_m \mathbf{\Psi}_{2m}, \qquad \text{on } R_2, \tag{46}$$

where N_1 is the number of nodes in region 1. Here, the vector $\mathbf{\Psi}_2$ holds those nodal values in the silencer section that lie in the airway (region R_2), including nodes with location y^- [for example, nodes *b* and *l* in Fig. 2(b)]. Similarly, vector $\mathbf{\Phi}_2$ holds those nodal values [for eigenfunction $\Phi(y,z)$] in the inlet duct that lie on transverse locations identical to locations chosen for the nodes making up $\mathbf{\Psi}_2$. This assumes that each node lying adjacent to a perforate in the silencer section also lies in the airway [for example, nodes *a* and *j* in Fig. 2(b)]. Thus, vectors $\mathbf{\Phi}_2$ and $\mathbf{\Psi}_2$ both have a length N_2. Continuity of axial velocity over plane A yields,

$$\sum_{j=0}^{N_1} F_j \gamma_j \mathbf{\Phi}_{2j} - \sum_{j=0}^{N_1} A_j \gamma_j \mathbf{\Phi}_{2j} = \sum_{m=0}^{N_c} B_m \lambda_m \mathbf{\Psi}_{2m} - \sum_{m=0}^{N_c} C_m \lambda_m \mathbf{\Psi}_{2m}, \qquad \text{on } R_2. \tag{47}$$

For plane B, continuity of pressure yields,

$$\sum_{m=0}^{N_c} B_m \mathbf{\Psi}_{2m} e^{-\mathrm{i}k_0 \lambda_m L} + \sum_{m=0}^{N_c} C_m \mathbf{\Psi}_{2m} e^{\mathrm{i}k_0 \lambda_m L} = \sum_{n=0}^{N_1} D_n \mathbf{\Phi}_{2n}, \qquad \text{on } R_2, \tag{48}$$

and continuity of axial particle velocity

$$\sum_{m=0}^{N_c} B_m \lambda_m \mathbf{\Psi}_{2m} e^{-\mathrm{i}k_0 \lambda_m L} - \sum_{m=0}^{N_c} C_m \lambda_m \mathbf{\Psi}_{2m} e^{\mathrm{i}k_0 \lambda_m L} = \sum_{n=0}^{N_1} D_n \gamma_n \mathbf{\Phi}_{2n}, \qquad \text{on } R_2. \tag{49}$$

For each splitter fairing, zero normal particle velocity over plane A yields,

$$\sum_{m=0}^{N_c} B_m \lambda_m \mathbf{\Psi}_{3m} - \sum_{m=0}^{N_c} C_m \lambda_m \mathbf{\Psi}_{3m} = \mathbf{0}, \qquad \text{on } R_3, \tag{50}$$

and for plane B,

$$\sum_{m=0}^{N_c} B_m \lambda_m \boldsymbol{\Psi}_{3m} e^{-\mathrm{i}k_0 \lambda_m L} - \sum_{m=0}^{N_c} C_m \lambda_m \boldsymbol{\Psi}_{3m} e^{\mathrm{i}k_0 \lambda_m L} = \mathbf{0}, \qquad \text{on } R_3. \tag{51}$$

Here, region R_3 encompasses all nodes that lie in the porous material, including nodes on a perforate with location y^+, so that vector $\boldsymbol{\Psi}_3$ has a length N_3. Finally, zero normal particle velocity over each splitter fairing is enforced for the inlet and outlet duct. Matching takes place over those nodes lying adjacent to region R_3, but does not include those nodes lying adjacent to a perforate. For example, in Fig. 2(b), conditions are enforced over nodes *h*, *f* and *d*. Thus, for plane A,

$$\sum_{j=0}^{N_1} F_j \gamma_j \boldsymbol{\Phi}_{3j} - \sum_{j=0}^{N_1} A_j \gamma_j \boldsymbol{\Phi}_{3j} = \mathbf{0}, \qquad \text{on } R_3, \tag{52}$$

and, for plane B

$$\sum_{n=0}^{N_1} D_n \gamma_n \boldsymbol{\Phi}_{3n} = \mathbf{0}, \qquad \text{on } R_3. \tag{53}$$

Here, vector $\boldsymbol{\Phi}_3$ contains all nodes adjacent to region R_3 except those lying on the perforate, so that vector $\boldsymbol{\Phi}_3$ has a length of $N_3 - N_p$, where N_p denotes the number of nodes positioned inside a splitter but adjacent to a perforate [nodes that have position y^+, for example nodes *c* and *k* in Fig. 2(b)]. Equations (46)-(53) form a complete set of $4(N_2 + N_3) - 2N_p$ equations (the collocation points) and $2(N_1 + N_c)$ unknowns (the modal amplitudes), since $N_1 = N_2 + N_3 - N_p$.

It is convenient to re-write Eqs. (46)-(53) and to introduce $\tilde{C}_m = C_m e^{-\mathrm{i}k_0\lambda_m L}$, to yield the final set of matching conditions:

$$\sum_{j=0}^{N_1} A_j \boldsymbol{\Phi}_{2j} - \sum_{m=0}^{N_c} B_m \boldsymbol{\Psi}_{2m} - \sum_{m=0}^{N_c} \tilde{C}_m \boldsymbol{\Psi}_{2m} e^{-\mathrm{i}k_0\lambda_m L} = -\sum_{j=0}^{N_1} F_j \boldsymbol{\Phi}_{2j}\,, \tag{54}$$

$$\sum_{j=0}^{N_1} A_j \gamma_j \boldsymbol{\Phi}_{2j} + \sum_{m=0}^{N_c} B_m \lambda_m \boldsymbol{\Psi}_{2m} - \sum_{m=0}^{N_c} \tilde{C}_m \lambda_m \boldsymbol{\Psi}_{2m} e^{-\mathrm{i}k_0\lambda_m L} = \sum_{j=0}^{N_1} F_j \gamma_j \boldsymbol{\Phi}_{2j}\,, \tag{55}$$

$$\sum_{m=0}^{N_c} B_m \lambda_m \boldsymbol{\Psi}_{3m} - \sum_{m=0}^{N_c} \tilde{C}_m \lambda_m \boldsymbol{\Psi}_{3m} e^{-\mathrm{i}k_0\lambda_m L} = \mathbf{0}\,, \tag{56}$$

$$\sum_{j=0}^{N_1} A_j \gamma_j \boldsymbol{\Phi}_{3j} = \sum_{j=0}^{N_1} F_j \gamma_j \boldsymbol{\Phi}_{3j}\,, \tag{57}$$

$$\sum_{m=0}^{N_c} B_m \boldsymbol{\Psi}_{2m} e^{-\mathrm{i}k_0\lambda_m L} + \sum_{m=0}^{N_c} \tilde{C}_m \boldsymbol{\Psi}_{2m} - \sum_{n=0}^{N_1} D_n \boldsymbol{\Phi}_{2n} = \mathbf{0}\,, \tag{58}$$

$$\sum_{m=0}^{N_c} B_m \lambda_m \boldsymbol{\Psi}_{2m} e^{-\mathrm{i}k_0\lambda_m L} - \sum_{m=0}^{N_c} \tilde{C}_m \lambda_m \boldsymbol{\Psi}_{2m} - \sum_{n=0}^{N_1} D_n \gamma_n \boldsymbol{\Phi}_{2n} = \mathbf{0}\,, \tag{59}$$

$$\sum_{m=0}^{N_c} B_m \lambda_m \boldsymbol{\Psi}_{3m} e^{-\mathrm{i}k_0\lambda_m L} - \sum_{m=0}^{N_c} \tilde{C}_m \lambda_m \boldsymbol{\Psi}_{3m} = \mathbf{0}\,, \tag{60}$$

$$\sum_{n=0}^{N_1} D_n \gamma_n \boldsymbol{\Phi}_{3n} = \mathbf{0}\,. \tag{61}$$

Equations (54)-(61) may be solved only after appropriate modal amplitudes F_j, which describe the incident sound field, have been specified. Source models are discussed in detail elsewhere (see for example, work by Kirby and Lawrie [10], Mechel [11], and Joseph *et al* [14]), although the most plausible representation of the noise emanating from a fan appears to be the assumption of equal modal energy density (EMED) for propagating modes. Accordingly, the inlet modal amplitudes, assuming EMED, are given as [11]

$$\left|\frac{F_j}{p_0}\right|^2 = I_0 \Big/ I_j \sum_{m=0}^{N_I} \gamma_m \,, \tag{62}$$

where p_0 is a reference pressure chosen here, arbitrarily, to be equal to unity; N_I is the number of modes propagating in the inlet duct (for modes that are "cut-off", $F = 0$), and

$$I_n = \int_{R_1} \left|\Phi_n(y,z)\right|^2 dydz \,. \tag{63}$$

Note that other source models, such as equal modal power, may readily be introduced here but are omitted in order to reduce the number of results presented later on. A finite element eigenvalue solution for the inlet duct yields an unordered list of eigenvalues, which are sorted and numbered so that $m = 0$ has the largest real part, $m = 1$ the second largest real part, and so on. Thus, Eq. (62) remains in general form, and the integral in Eq. (63) is computed numerically. After determining appropriate values for F_j, Eqs. (54)-(61) are solved simultaneously to find the $2(N_1 + N_c)$ unknown modal amplitudes.

A common method for representing silencer performance is the silencer transmission loss (*TL*), which is defined as the ratio of transmitted to incident sound powers (note that for experimental measurements undertaken according to ISO standards [15], the transmission loss of a silencer is equivalent to the insertion loss). The inlet sound power is equal to unity, hence, in decibels

$$TL = -10\log_{10} \sum_{n=0}^{N_I} \frac{\gamma_n I_n \left|D_n\right|^2}{I_0} \,. \tag{64}$$

III. RESULTS AND DISCUSSION

The addition of higher-order incident modes aims to replicate the incident sound pressure field typically present in a real HVAC ducting system. The measurement of silencer performance, when placed *in situ*, does, however, present many difficulties, not least in accurately measuring the sound pressure field emitted by a fan. To overcome these difficulties, laboratory measurements for splitter silencers are normally performed using plane wave excitation. For example, the measurements reported by Mechel [12] were performed according to standards (see also BS 7235 [15]) that stipulate an incident sound field with "dominating plane wave mode". Accordingly, comparison between prediction and experiment is restricted here to transmission loss curves measured under plane wave excitation; the proposed model for multi-modal excitation is investigated theoretically and reported separately.

The absorbent material in each splitter is assumed to be fibrous and bulk reacting. Accordingly, the generalised results of Delany and Bazley [16], yield

$$\Gamma = 0.189\xi^{-0.595} + \mathrm{i}\left(1 + 0.098\xi^{-0.7}\right) \tag{65}$$

for the propagation constant, and

$$\rho(\omega) = -\rho_0\Gamma\left[0.087\xi^{-0.732} + \mathrm{i}\left(1 + 0.057\xi^{-0.754}\right)\right] \tag{66}$$

for the complex density. Here, ξ is a non-dimensional frequency parameter given by $\xi = \rho_0 f/\sigma$, where f is frequency and σ is the flow resistivity of the porous material. The formulae of Delany and Bazley are known to be invalid at low frequencies, and so the semi-empirical correction formulae of Kirby and Cummings [17] (see also Ref. [13]) are adopted here to alleviate this inconsistency. Note that this method replicates, as far as possible, Delany and Bazley's regression formulas over the frequency range for which their data is known to be valid; outside of this frequency range, plausible limiting values are substituted. The theoretical analysis presented here is, however, sufficiently general so that alternative models for the porous material may be substituted (see, for example, alternative models suggested by Wilson [18] and Allard and Champoux [19]). The impedance of the perforate is given as [13],

$$\zeta = \left[\zeta' - 0.425\mathrm{i}k_0 d_p\left(\rho(\omega)/\rho_0 - 1\right)\right]/\Omega\,, \tag{59}$$

where

$$\zeta' = \left[1 + t/d_p\right]\sqrt{8k_0\nu/c_0} + \mathrm{i}k_0 d_p\left[0.25 + t/d_p\right]. \tag{60}$$

Here, t is the thickness of the perforate, d_p is the hole diameter, Ω is the perforate area porosity, and ν is the kinematic viscosity of air.

A. Plane wave excitation

The experimental data reported by Mechel [12] are used here in order to compare prediction with experiment. The assumption of plane wave excitation greatly simplifies the analysis since silencer symmetry may be utilised in order to reduce the problem from three to two dimensions (x, y plane). Accordingly, the silencers tested by Mechel [12] may be simplified and a duct lined

on opposite walls analysed. Mechel examined five different silencer configurations, for which each splitter contained an end fairing, although no perforate was present. Only three of the five silencer configurations reported by Mechel are studied here, as this is deemed sufficient to evaluate the current analysis. The dimensions of each silencer, after accounting for lines of symmetry, are listed in Table I. A comparison between the measurements of Mechel [12] and predictions for silencer A is shown in Fig. 3. Predictions are shown with and without splitter fairings (see Ref. [10] for an equivalent model that omits splitter fairings) and for a high perforate porosity ($\Omega = 0.95$) so that any effects of the perforate in the current analysis are negligible. Agreement between prediction and experiment in Fig. 3 is good, although in the medium frequency range some discrepancies are evident. Agreement is similar to that reported by Mechel [12], who assumes a locally reacting liner, although for the medium frequency range the current method tends to over predict transmission loss, whereas Mechel under predicts transmission loss. The good agreement between the two methods at low and high frequencies suggests that, at these frequency extremes, performance depends strongly on the silencer geometry. Moreover, the effect of adding splitter fairings is clearly evident, although only within the medium frequency range, which further supports this observation. The peak in transmission loss seen for silencer A (and also for silencers B and C to follow) is caused by the cut-on of the (0, 2) mode in regions R_1 and R_4. Such a peak in transmission loss is observed only in studies of finite length HVAC silencers (that include the inlet/outlet ductwork) and may be seen also in the predictions of Mechel [12].

The material in silencer B has a higher flow resistivity than that in silencer A, and also a smaller cross-sectional area. Figure 4 reveals a maximum discrepancy of about 4 dB between prediction

and experiment, although the current model again over predicts silencer performance in the medium frequency range. Here, direct comparison between prediction and experiment is difficult as the experiment adopts a one third octave band analysis, whereas predictions are narrow band. Hence, experimental measurements are unlikely to exhibit the marked peaks seen in predicted transmission loss. Mechel [12] does, however, appear to obtain better agreement for this silencer at frequencies close to 1 kHz, although again the silencer transmission loss is under predicted.

For silencers A and B, consistent differences between the current model and that of Mechel [12] exist: the current model tends to over predict transmission loss, whereas Mechel tends to under predict transmission loss, especially in the medium frequency range. This difference is not surprising given that Mechel suppresses sound propagation in the material itself. However, neither method accurately reproduces experimental measurements over the whole frequency range, even though the current method properly represents the propagation of sound within the absorbing material. The accuracy of predictions do, however, compare well with those reported for dissipative automotive exhaust silencers, especially if one takes into account the relative complexity of the current silencer. It is possible that the differences observed between the current predictions and experimental measurements may partly be explained by inaccurate characterisation of the absorbing material: the bulk acoustic properties are based here on the Delany and Bazley coefficients [16] averaged over a number of fibrous materials, and these may not accurately represent the performance of an individual real material. Note that the material data referred to by Mechel [12] was also obtained after averaging measurements over a number of fibrous materials and predictions are very similar to those found when using Delany and

Bazley's coefficients. Furthermore, discrepancies at medium and high frequencies may by caused by neglecting the effects of structural flanking transmission, which may appear in the form of noise bypassing the silencer and travelling along the duct walls or, alternatively, breaking out of the test duct and breaking back in downstream of the silencer.

Silencer C has a more extreme geometry as the airway takes up only 20% of the overall cross-sectional area. Comparison between prediction and experiment in Fig. 5 shows discrepancies that are far more pronounced than for silencers A and B, especially above 1 kHz. Mechel [12] observed similar discrepancies, and both methods significantly over predict silencer performance at higher frequencies. Mechel proposed that assuming a locally reacting material caused these discrepancies. The current analysis addresses this issue by treating the material as bulk reacting, although it is evident in Fig. 5 that agreement with measured data has not significantly been improved. Thus, at higher frequencies the model used for the porous material cannot explain discrepancies; instead, it is highly likely that these differences are caused by structural flanking transmission. Cummings and Astley [20] investigated this effect for lined ducts and showed that flanking transmission places limits on silencer performance. They note also, "If the silencer presents a large attenuation (at a particular frequency) to the internal sound field, especially by virtue of its length, there is a possibility that flanking paths may exist, resulting in loss of acoustic performance". Furthermore, Brandstätt *et al.* [9] examine silencers similar to those studied here, and use experimental techniques that are likely to be similar to those used by Mechel [12] (given the commonality in institutions between the lead authors). Brandstätt *et al.* acknowledge that flanking transmission may limit the attenuation values measured for their silencers, although they postulate that this effect is limited only to the medium frequency range

(around 1 kHz). Brandstätt *et al.* further suggest that discrepancies between prediction and experiment at higher frequencies are caused by "reflection at the splitter, but also…higher-order modes in the air passage which are well attenuated". However, current results – that include all relevant duct modes - do not support the latter of these observations, as predictions lie above measured transmission loss values at higher frequencies. Instead, current results support the observations of Cummings and Astley [20] since a loss of silencer performance is observed at regions of high attenuation and this includes in the higher frequency range. Accordingly, the omission of structural flanking transmission limits the applicability of the current approach, at least for silencers that present a large attenuation at a particular frequency.

B. Multi-mode excitation

In HVAC ducts a multi-mode incident sound field, driven by the fan, is likely to be present above the cut-on frequency of the first higher order duct mode. It is normal to assume that these higher order modes share a common property, for example, equal modal energy density (EMED) [11, 14]. Modelling a multi-mode incident sound field does, however, require a fully three-dimensional approach, as lines of symmetry no longer exist [11]. Accordingly, a two-dimensional eigenvalue analysis (y, z plane) is necessary and this incurs a significant increase in computational expenditure when compared to the one-dimensional eigenvalue (y plane) approach suitable for plane wave excitation.

The effect of an EMED incident sound field on the acoustic performance of silencer C is shown in Fig. 5 (assuming a representative duct height of 0.4 m, as Mechel [12] did not publish values

of H for his test silencers). For this silencer, transmission loss predictions are generally lower than for plane wave excitation. This behaviour is likely to be caused by higher order modes propagating at angles that bypass the splitter fairings. This effect depends on silencer geometry and frequency, as well as the choice of absorbing material, although it is possible, under some circumstances, for the splitter fairings to preferentially reflect higher order modes.

The multi-mode predictions for silencer C were generated using a transverse mesh refined according to excitation frequency. As frequency increases it's normal to increase the number of degrees of freedom in the finite element mesh: as a general guideline, between 7 and 10 finite element nodes should be adopted per wavelength [21]. Thus, for HVAC silencers a very large number of degrees of freedom are often necessary, even for relatively small silencers. For example, at 2 kHz, values of $N_1 = 533$ and $N_c = 585$, were found to be necessary for silencer C; at 4 kHz double this number are required. It is clear that matrix dimensions can quickly become very large for multi-mode excitation, and transmission loss predictions for silencer C stop at 4 kHz in Fig. 5 because of computational limitations. Furthermore, at higher frequencies the number of propagating incident modes becomes very large: at 4 kHz, 96 modes are found to propagate. Many of these incident modes have very similar wavenumbers and numerical problems arise if these modes are not accurately computed. In a real HVAC duct it is, however, unlikely that this number of incident modes will propagate at higher frequencies, and the usefulness of adopting EMED is probably limited at higher frequencies.

The computational expenditure associated with modelling three-dimensional sound propagation encourages an investigation into the feasibility of approximating silencer performance using a

two-dimensional approach. In Fig. 6 comparison between predictions generated with and without the assumption of cross-sectional symmetry are shown for a splitter silencer (silencer D, see Table I) that represents silencers typically found in HVAC systems. Silencer D contains both a perforate and splitter fairings: for the perforate, $t = 1\,\text{mm}$, $d_p = 3.5\,\text{mm}$, and $\Omega = 0.3$. Transmission loss predictions shown in Fig. 6 were generated using a two-dimensional representation of the splitter (*x*, *y* axis), for $0 \le y \le b$, and $0 \le y \le b/2$, and these are compared against a three-dimensional solution. Silencer D is larger than silencer C and computational resources restrict predictions for the three-dimensional approach to a maximum frequency of 2 kHz (where, $N_1 = 633$ and $N_c = 765$). A comparison between two- and three-dimensional predictions shows reasonably good agreement and generally the predictions are within 10 dB of one another. It is evident that the two-dimensional model, encompassing $0 \le y \le b$, produces better agreement with three-dimensional predictions, when compared to the model encompassing $0 \le y \le b/2$; this is to be expected, as a greater number of incident modes are included in the former model. Although the level of agreement between two- and three-dimensional formulations will depend on the particular silencer chosen, after analysing a number of different splitter silencers (not shown here) the predictions shown in Fig. 6 appear to be representative of the general level of agreement to be expected. Therefore, it appears sensible, at least in the preliminary stages of an iterative design procedure, to adopt a two-dimensional model for a splitter silencer, even if the silencer is excited by higher order modes. Accordingly, all further results presented here were obtained using a two-dimensional representation (*x*, *y* plane) of the splitter silencer.

It is interesting to examine the effect of splitter fairings on the sound pressure distribution in the duct. For silencer D, the relative sound pressure level at a frequency of 1.5 kHz, calculated using a two dimensional ($0 \le y \le b/2$) representation, is shown with splitter fairings in Fig. 7, and without fairings in Fig. 8. The influence of the fairings on sound pressure distribution is most obvious in the inlet duct, especially close to the inlet plane of the silencer. It is interesting also to note that the sound pressure fields, downstream of the silencer, are similar to one another in Figs. 7 and 8, especially well away from the silencer outlet plane. Moreover, the complex nature of this sound pressure field demonstrates the difficulty in measuring accurately silencer performance when higher order modes propagate downstream of the silencer.

The influence of perforate porosity on silencer transmission loss is shown, for silencer D, in Fig. 9. Here, the same perforate porosity is used for each baffle and it's evident that, as the perforate area porosity is reduced, the transmission loss increases slightly at low frequencies but reduces significantly at higher frequencies. This behaviour is similar to that found by other authors [1, 13] and indicates that, at least for larger HVAC silencers, it is preferable to use perforates with a high percentage open area. The model developed in Sec. II also allows for a different perforate porosity to be used for each splitter. By altering perforate porosity it is possible to manipulate the transmission loss curves shown in Fig. 9, although after conducting a number of numerical tests an improvement in transmission loss, over and above that found for a nominal limiting value of $\Omega = 0.4$, was not forthcoming. Similarly, it is straightforward to alter the material properties for each splitter section, however after a number of parametric studies only relatively minor modifications in silencer performance were observed – predominantly in the medium frequency range. Moreover, such modifications in performance depend heavily on the silencer

geometry chosen, which prevents the formulation of general guidelines regarding the optimum choice of material properties in splitters.

Transmission loss predictions obtained in the absence of splitter fairings and a perforate [see Kirby and Lawrie [10]) are also shown in Fig. 9. It is clear that splitter fairings have a significant effect on silencer performance and, for the silencers studied here, the effect of splitter fairings is more noticeable when higher order modes are present in the inlet duct.

IV. CONCLUSIONS

A two-dimensional analysis for a splitter silencer provides reasonable agreement with results obtained using a three-dimensional model. The largest discrepancy between the two methods is in the medium frequency range. The computational savings found when using the two-dimensional model are significant and it appears preferable to adopt a two-dimensional model, at least for a preliminary iterative design procedure.

Results indicate that, for splitter silencers, it is preferable to adopt as high a perforate porosity as possible and that no significant improvement in performance can be obtained by varying the porosity for different baffles. General guidelines do not, however, readily present themselves when it comes to the choice of absorbing material for each splitter. Moreover, at low and high

frequencies silencer performance largely depends on silencer geometry rather than the type of material chosen.

Splitter fairings significantly affect HVAC silencer performance. This effect is most noticeable in the medium frequency range, and when the silencer is excited by higher order modes. Thus, laboratory measurements, or theoretical predictions, based on a predominantly plane wave sound source are unlikely to represent accurately the performance of a silencer in a real ducting system. Moreover, structural flanking effects may also limit both the accuracy of the current modelling approach, and also the applicability to real systems of silencer measurements taken under laboratory conditions (in which structural flanking has been suppressed).

REFERENCES

1. A. Cummings, "Sound attenuation in ducts lined on two opposite walls with porous material, with some application to splitters," J. Sound Vib. **49**, 9-35 (1976).
2. D.A. Bies, C.H. Hansen and G.E. Bridges, "Sound attenuation in rectangular and circular cross-section ducts with flow and bulk-reacting liner," J. Sound Vib. **146**, 47-80 (1991).
3. S.K. Kakoty and V.K. Roy, "Bulk reaction modeling of ducts with and without mean flow," J. Acoust. Soc. Am. **112,** 75-112 (2002).
4. A. Cummings and N. Sormaz, "Acoustic attenuation in dissipative splitter silencers containing mean fluid flow," J. Sound Vib. **168**, 209-227 (1993).
5. R.J. Astley and A. Cummings, "A finite element scheme for attenuation in ducts lined with porous material: comparison with experiment," J. Sound Vib. **116**, 239-263 (1987).
6. R. Ramakrishnan and W.R. Watson, "Design curves for rectangular splitter silencers," Appl. Acoust. **35**, 1-24 (1992).
7. R. Ramakrishnan and R. Stevens, "Improving the accuracy of duct insertion loss predictions," J. Sound Vib. **169**, 423-427 (1994).
8. L.L. Beranek, *Noise and Vibration Control* (McGraw-Hill, New York, 1971).
9. P. Brandstätt, W. Frommhold and M.J. Fisher, "Program for the computation of absorptive silencers in straight ducts," Appl. Acoust. **43**, 19-38 (1994).
10. R. Kirby and J.B. Lawrie, "A point collocation approach to modelling large dissipative silencers," J. Sound Vib. to appear.
11. F.P. Mechel, "Theory of baffle-type silencers," Acustica **70**, 93-111 (1990).

12. F.P. Mechel, “Numerical results to the theory of baffle-type silencers,” Acustica **72**, 7-20 (1990).
13. R. Kirby, “Transmission loss predictions for dissipative silencers of arbitrary cross section in the presence of mean flow,” J. Acoust. Soc. Am. **114,** 200-209 (2003).
14. P. Joseph, C.L. Morfey and C.R. Lowis, “Multi-mode sound transmission in ducts with flow,” J. Sound Vib. **264**, 523-544 (2003).
15. European Standard EN ISO 7235, “Measurement procedures for ducted silencers – insertion loss, flow noise and total pressure loss,” (2003).
16. M.E. Delany and E.N. Bazley, “Acoustical properties of fibrous materials,” Appl. Acoust. **3**, 105-116 (1970).
17. R. Kirby and A. Cummings, “Prediction of the bulk acoustic properties of fibrous materials at low frequencies,” Appl. Acoust. **56**, 101-125 (1999).
18. D.K. Wison, “Simple, relaxational models for the acoustical properties of porous media,” Appl. Acoust. **50**, 17-188 (1997).
19. J.-F. Allard and Y. Champoux, “New empirical equations for sound propagation in rigid frame fibrous materials,” J. Acoust. Soc. Am. **91,** 3346-3353 (1992).
20. A. Cummings and R.J. Astley, “Effects of flanking transmission on sound attenuation in lined ducts,” J. Sound Vib. **179**, 617-646 (1995).
21. R.J. Astley, “Finite elements in acoustics,” *Proceedings of Internoise 98*, Christchurch, New Zealand, 1998.

Table I.
Data for silencers.

Silencer	d_1 (m)	h_1 (m)	d_2 (m)	h_2 (m)	d_3 (m)	L (m)	H (m)	σ (Pa s /m^2)
A	0.18	0.24	0.18	-	-	1.5	-	11000
B	0.1	0.2	0.1	-	-	0.5	-	12500
C	0.1	0.05	0.1	-	-	0.5	-	12500
D	0.1	0.1	0.2	0.1	0.1	0.9	0.9	8000

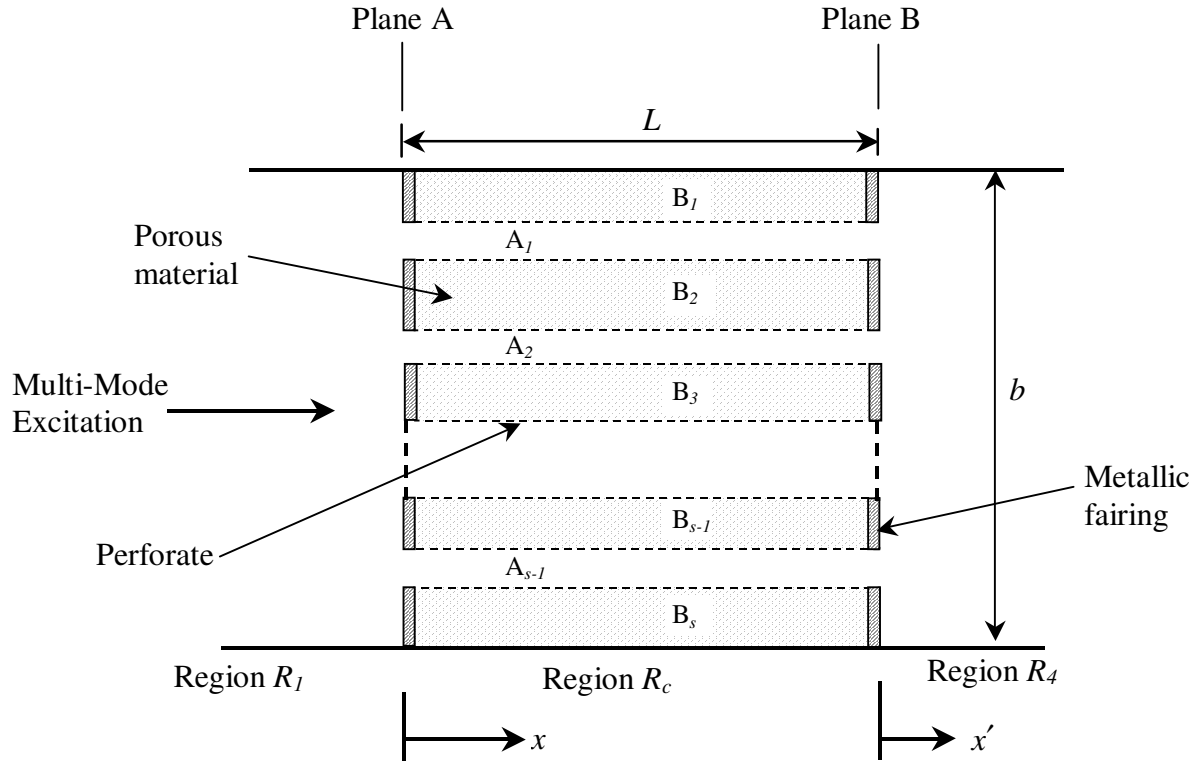

(a)

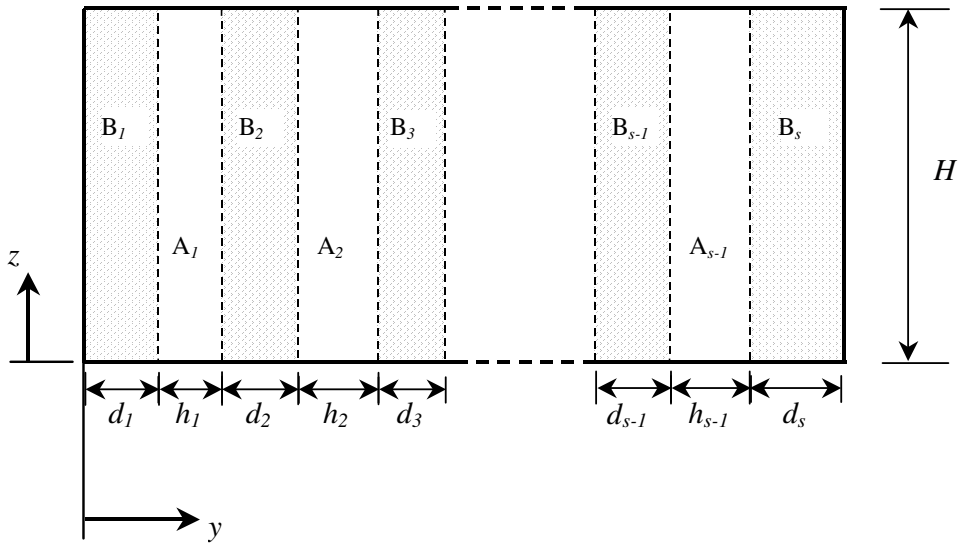

(b)

Fig. 1. (a) Plan view of silencer geometry (a splitter consists of a section of porous material that is bounded at either end by a metallic fairing, and separated from the airway by a perforated sheet). (b) Geometry of silencer cross-section.

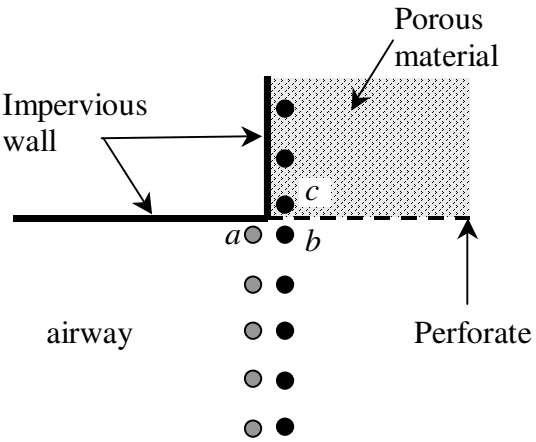

(a)

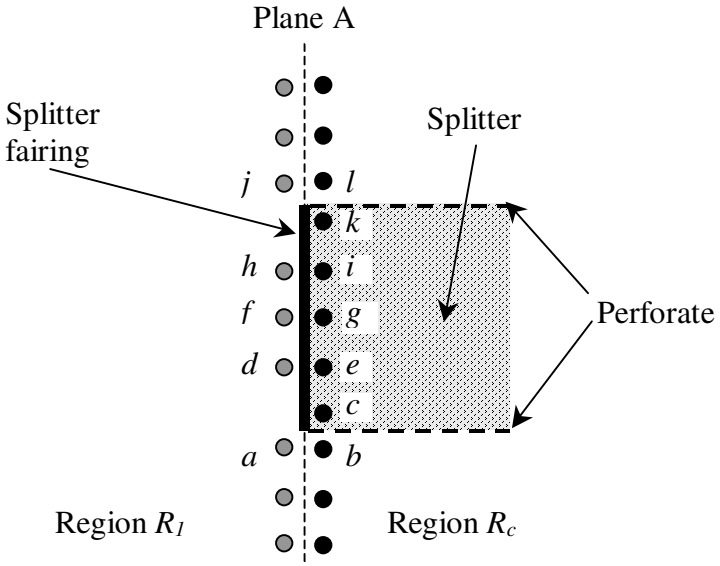

(b)

Fig. 2. (a) Example of nodal locations near a perforate for an automotive silencer [13]. (b) Example of nodal locations for a single splitter.

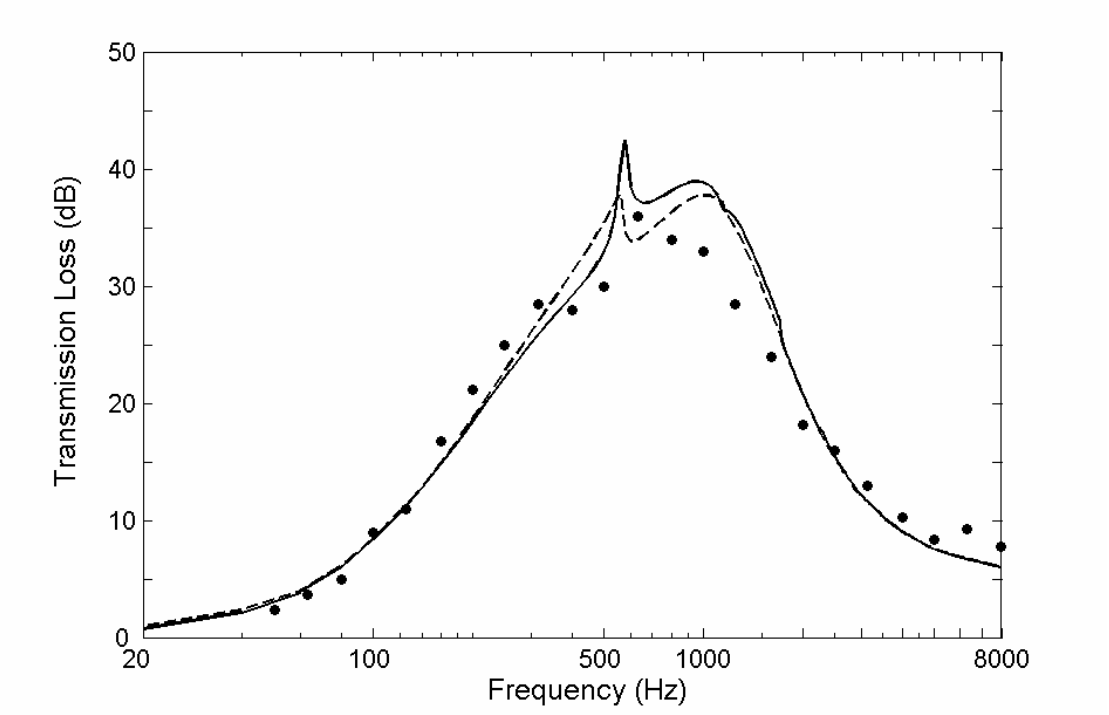

Fig. 3. Transmission loss for silencer A: ●, experiment [12]; ———, prediction with fairings ($N_1 = 41, N_c = 43$); — — —, prediction without fairings ($N_1 = N_c = 41$).

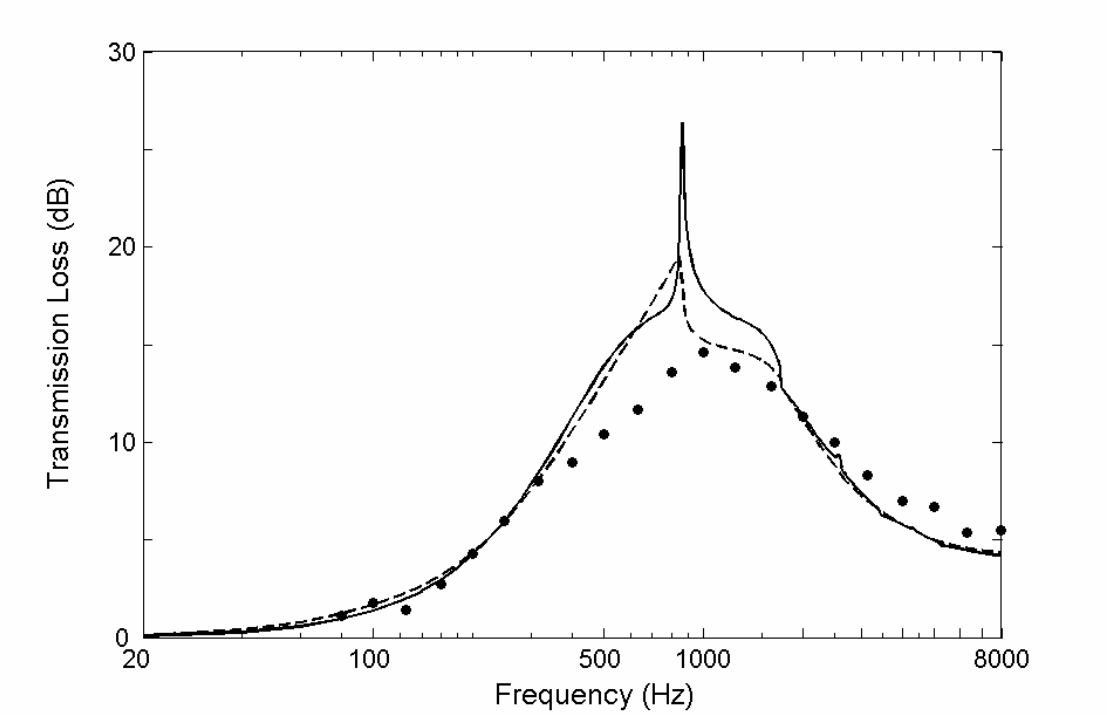

Fig. 4. Transmission loss for silencer B: ●, experiment [12]; ———, prediction with fairings ($N_1 = 33, N_c = 35$); — — —, prediction without fairings ($N_1 = N_c = 33$).

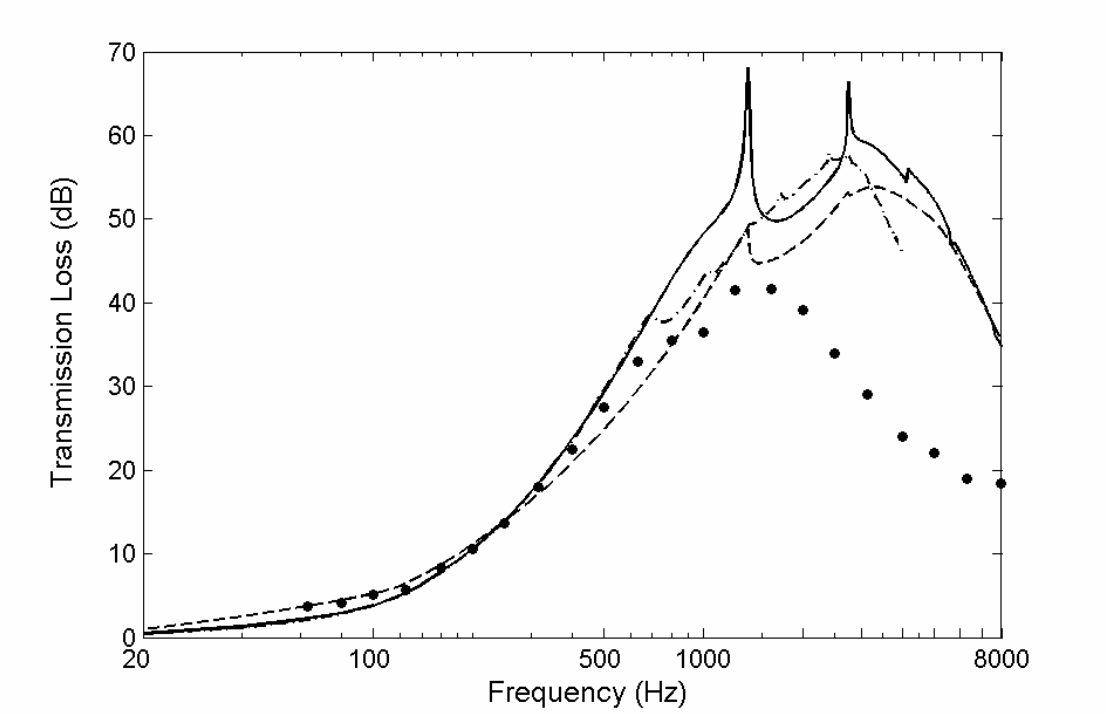

Fig. 5. Transmission loss for silencer C: ●, experiment [12]; ———, prediction with fairings ($N_1 = 21, N_c = 23$); — — —, prediction without fairings ($N_1 = N_c = 21$); — - — - —, three dimensional model, EMED excitation, prediction with fairings ($N_1 = 533, N_c = 585$).

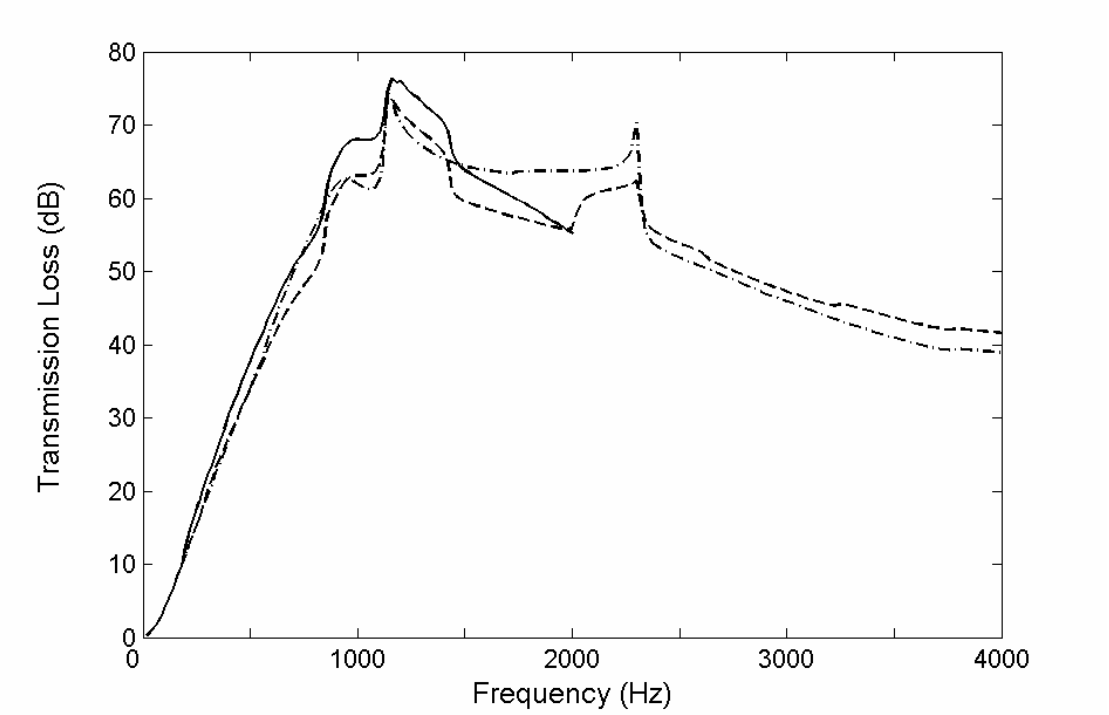

Fig. 6. Transmission loss predictions for silencer D with EMED excitation: ———, three-dimensional model; — — —, two-dimensional model for $0 \le y \le b$ ($N_1 = 25, N_c = 29$); — - — - —, two-dimensional model for $0 \le y \le b/2$ ($N_1 = 13, N_c = 15$).

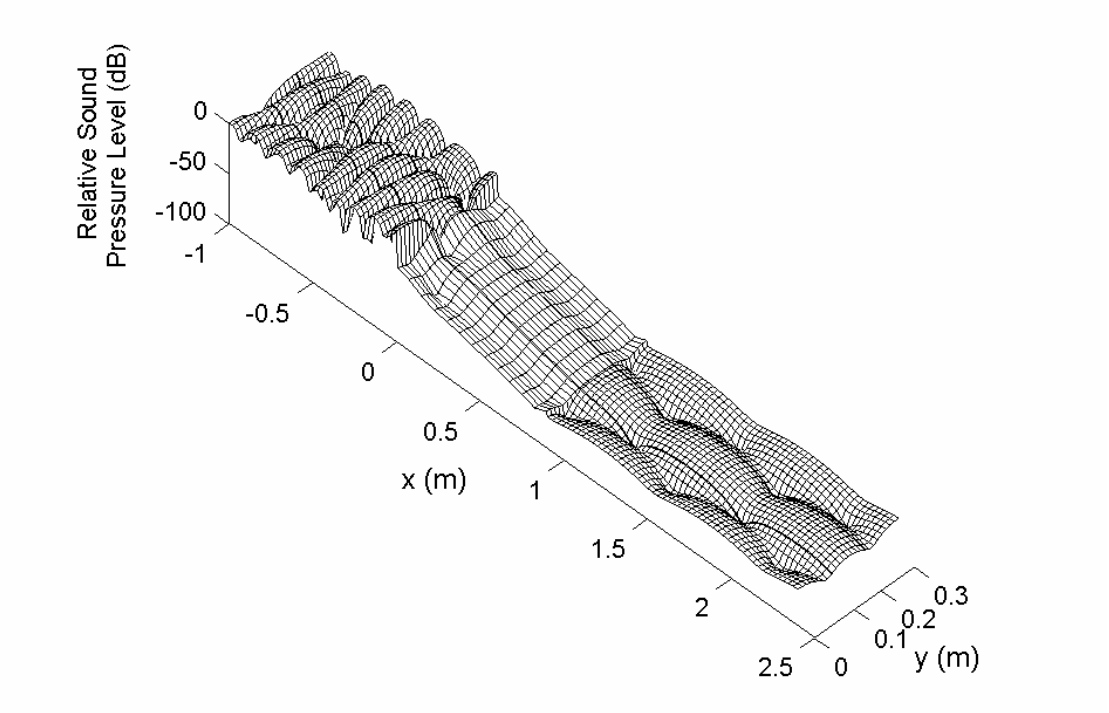

Fig. 7. Sound pressure distribution at 1500 Hz for silencer D with splitter fairings, $0 \le y \le b/2$.

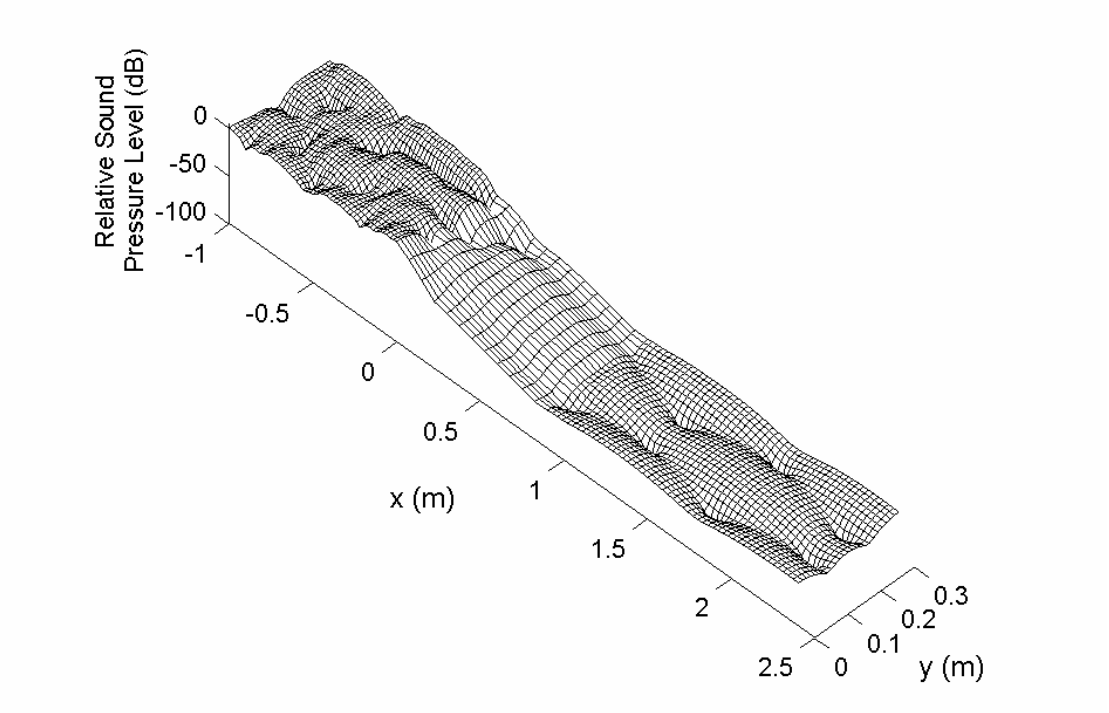

Fig. 8. Sound pressure distribution at 1500 Hz for silencer D without splitter fairings, $0 \le y \le b/2$.

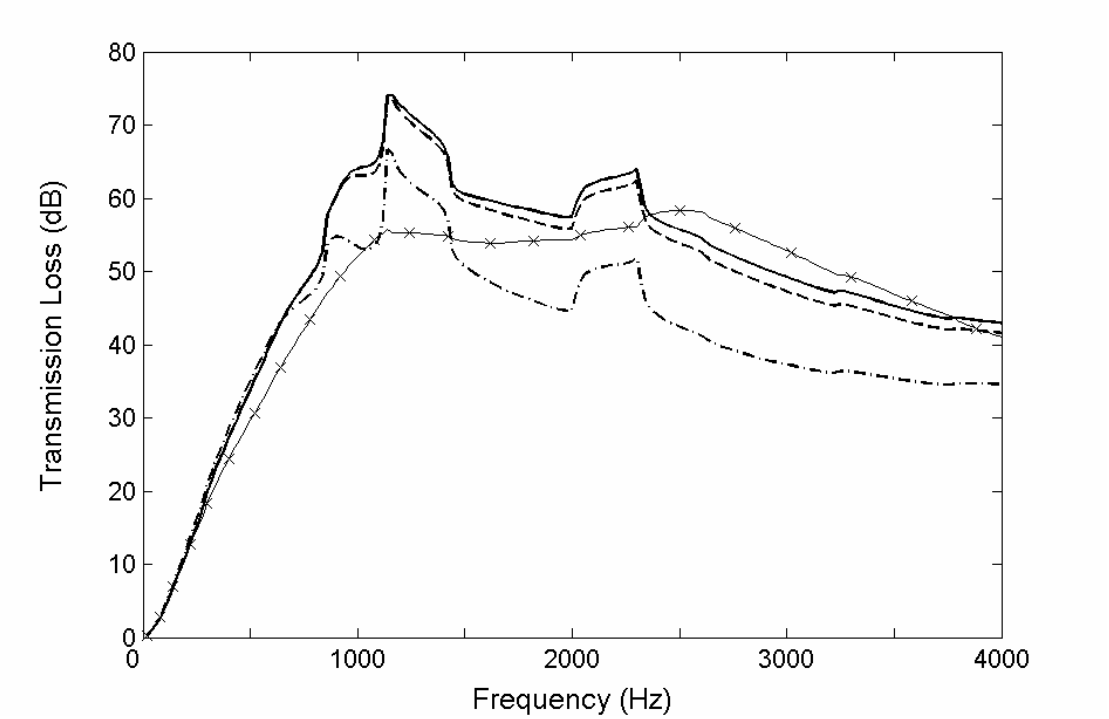

Fig. 9. Transmission loss predictions for silencer D with EMED excitation ($N_1 = 25, N_c = 29$): ————, $\Omega = 0.4$ with splitter fairing; — — —, $\Omega = 0.3$ with splitter fairing; — - — - —, $\Omega = 0.1$ with splitter fairing; —×—×—, without perforate and fairing.